Evaluation of Polar WRF forecasts on the Arctic System Reanalysis domain: Surface and upper air analysis

Aaron B. Wilson,[1,2] David H. Bromwich,[1,2] and Keith M. Hines[1]

Received 3 September 2010; revised 11 March 2011; accepted 18 March 2011; published 9 June 2011.

[1] The Polar version 3.1.1 of the Weather Research and Forecasting model (WRF), a high-resolution regional scale model, is used to simulate conditions for the year December 2006 to November 2007. The goal is to compare model output of near-surface and tropospheric variables to observational data sets. The domain mirrors that of the Arctic System Reanalysis (ASR), an assimilation of model fields with Arctic observations being conducted partly by the Polar Meteorology Group of the Byrd Polar Research Center at Ohio State University. A key development in this Polar WRF study is the extension of the seasonal progression of sea ice albedo to the entire Arctic Ocean. The boundary conditions are specified by the NCEP Final global gridded analysis archive (FNL), a 1° × 1° global grid updated every 6 h. The simulations are performed in 48 h increments initialized daily at 0000 UTC, with the first 24 h discarded for model spin-up of the hydrologic cycle and boundary layer processes. Model large-scale variables of atmospheric pressure and geopotential height show good agreement with observations. Spatial distribution of near-surface air temperatures compares well with ERA-Interim despite a small negative bias in the station analysis. Surface dewpoint temperatures and wind speeds show small biases, but model skill is modest for near-surface winds. Tropospheric temperatures and wind speeds, however, agree well with radiosonde observations. This examination provides a benchmark from which to improve the model and guidance for further development of Polar WRF as ASR's primary model.

Citation: Wilson, A. B., D. H. Bromwich, and K. M. Hines (2011), Evaluation of Polar WRF forecasts on the Arctic System Reanalysis domain: Surface and upper air analysis, *J. Geophys. Res.*, *116*, D11112, doi:10.1029/2010JD015013.

1. Introduction

[2] A current challenge is to merge various forms of information about the Arctic being collected for climate change purposes (e.g., field observations, satellite data, and model output). While Global Climate Models (GCMs) are being extensively used for climate change projections into the 21st century, higher resolution regional-scale models have become a necessary tool for analyzing and predicting weather and climate in the Arctic. As a result of the Study of Environmental Arctic Change (SEARCH) [*Arctic Research Consortium of the United States*, 2005], the Arctic System Reanalysis (ASR) [*Bromwich et al.*, 2010] is being performed. ASR is the merging of historical atmospheric, oceanic, land surface, and cryosphere observations using data assimilation techniques and regional modeling with the goal of enhanced understanding of the Arctic's atmosphere/sea ice/land system.

[3] As part of this Arctic integration effort, research and development of a high resolution regional scale atmospheric model, specifically the Weather Research and Forecasting Model (WRF) [*Skamarock et al.*, 2008], is being conducted by the Polar Meteorology Group at the Byrd Polar Research Center of Ohio State University. Modifications to WRF for polar applications have been ongoing, with the intent of designing an Arctic friendly mesoscale model to be used as the primary model for ASR.

[4] A series of highly detailed analyses of regional modeling with Polar WRF have been performed with results compared to selected local observations. Polar WRF was first tested over the Greenland ice sheet using version 2.1.1 [*Hines and Bromwich*, 2008] and led to improvements of the 4-layer Noah Land Surface Model (LSM) [*Chen and Dudhia*, 2001]; updates were made to longwave emissivity, upward longwave flux, deep snowpack treatment, and thermal conductivity of permanent ice and snow surfaces. Next, Polar WRF was tested over the Arctic Ocean in order to improve the surface treatment of sea ice [*Bromwich et al.*, 2009]. Polar WRF version 2.2 was evaluated against observations made at the drifting station SHEBA [*Perovich et al.*, 1999; *Uttal et al.*, 2002]. Fractional sea ice was implemented, specifying conditions associated with ice and open-water areas of sea ice grid boxes. Likewise, sea ice albedo was set as a function time

[1]Polar Meteorology Group, Byrd Polar Research Center, Ohio State University, Columbus, Ohio, USA.
[2]Atmospheric Sciences Program, Department of Geography, Ohio State University, Columbus, Ohio, USA.

0148-0227/11/2010JD015013

and latitude to account for the strong seasonal cycle. Finally, Polar WRF was tested over Arctic land using version 3.0.1.1 and compared to observations from the North Slope of Alaska [*Hines et al.*, 2011]. A sensitivity study using reduced soil heat conductivity was used during a January 2007 simulation in order to improve near surface air temperatures, which were previously too warm. Additionally, summer simulation of longwave and shortwave radiation showed a presumed underrepresentation of Arctic stratus clouds over land, with excessive incident shortwave radiation.

[5] While the near-surface results of Polar WRF performance over the Greenland ice sheet, sea ice, and Arctic land have been analyzed, Polar WRF has not been thoroughly examined on the full ASR domain. In particular, the performance in the middle and upper troposphere, that are especially sensitive to the synoptic and larger scales, has not been documented. Thus, to prepare for the ASR, this macroscale study analyzes short-term forecasts from the optimized Polar WRF model used as the base model for ASR. The domain includes the immediate Arctic region, the surrounding river basins, and lower latitudes, and interest lies in optimizing performance over the Arctic without penalizing it in other areas. The year selected for analysis is December 2006–November 2007, the year of record sea ice minimum extent [*National Snow and Ice Data Center*, 2007]. This analysis focuses on the surface and upper air performance of Polar WRF, while a companion paper will analyze Polar WRF's atmospheric hydrologic cycle. Does the optimized high resolution mesoscale model Polar WRF predict with a high degree of realism the physical atmospheric processes that occur in the Arctic and midlatitudes? Section 2 describes the Polar WRF configuration used in this investigation. Section 3 depicts the model domain and input data and the following section describes the data sets used for validation. Sections 5 and 6 detail the results of the surface analysis while sections 7 and 8 highlight upper-level performance. Finally, a summary is provided in section 9.

2. Polar WRF Configuration and Dynamics

[6] For this investigation, the polar version of WRF 3.1.1 is used. This adapted version of Polar WRF uses 39 vertical terrain following sigma levels from the Earth's surface to 10 hPa, with the lowest layer centered at 8 m AGL. It has been demonstrated that a higher model top provides better treatment of upward propagating gravity waves [*Bromwich et al.*, 2005]. Likewise, additional damping of the top 8 km of the model is utilized through a diffusion option.

[7] Long-term uninterrupted limited area simulations suffer from a build up of errors over time despite updated lateral boundary conditions [*Lo et al.*, 2008]. Therefore "forecast mode" is implemented here with 48 h simulations initialized daily at 0000 UTC allowing for model "spin-up." Two aspects of the model atmosphere require spin-up: the hydrologic cycle and the planetary boundary layer (PBL). Past experience with the Antarctic boundary layer shows the PBL becomes quasi-steady after 12 h of spin-up [*Parish and Waight*, 1987; *Parish and Bromwich*, 1991; *Parish*, 1992; *Parish and Cassano*, 2003]. While 12 h spin-up was chosen for Greenland-area Polar WRF simulations [*Hines and Bromwich*, 2008], the subsequent studies of the Arctic Ocean and Arctic land utilized 24 h spin-up as it was thought a 24 h minimum forecast time would provide a slightly more difficult challenge for the model. The 24 h spin-up therefore is retained for this current study. All 3 hourly model outputs are compiled and compared to 3 hourly observations for the annual cycle.

[8] For this study, many of the physics parameterizations have been chosen in light of previous Polar WRF experiments described in the introduction. For the cloud microphysics parameterization the WRF single moment 6-class scheme is used [*Hong and Lin*, 2006]. Having been successfully tested in the Greenland simulation, this scheme allows vapor, rain, snow, cloud ice, graupel, and cloud supercooled water, as well as a gradual melting for snow falling through a melting layer. The cumulus parameterization in Polar WRF is provided by the new Grell-Devenyi 3D ensemble scheme [*Skamarock et al.* 2008], based on an older version [*Grell and Devenyi*, 2002]. Here, multiple cumulus schemes are run within each grid box and the results are averaged and provided to the model. Likewise, each grid box handles the entrainment and detrainment processes separately. For the PBL, the Mellor-Yamada-Janjic (MYJ) [*Janjić*, 2002] scheme has been chosen providing a parameterization of the turbulence in the PBL and free atmosphere. Equally important, it has been demonstrated in Polar WRF's Greenland simulation to perform as well as other PBL schemes [*Hines and Bromwich*, 2008]. With regard to atmospheric radiation parameterizations, the Rapid Radiative Transfer Model (RRTM) [*Mlawer et al.*, 1997] scheme and the Goddard Shortwave [*Chou and Suarez*, 1994] scheme are implemented for longwave and shortwave radiation, respectively. The RRTM parameterizes longwave processes involved with water vapor, ozone, CO_2, and trace gases. Additionally, the RRTM has been found to be superior to other longwave radiation schemes for previous simulations of Arctic environments in the treatment of longwave energy during clear-sky conditions [*Inoue et al.*, 2006; *Pinto et al.*, 1997; *Ruffieux et al.*, 1995]. Recent evidence suggests the RRTM scheme in WRF may lead to excessive cooling in the upper levels near the model top [*Powers et al.*, 2010]. However, this analysis is restricted to levels at or below 100 hPa, and the new RRTMG scheme is not explored.

[9] For the land surface, the Noah LSM (updates described in section 1) with an Eta similarity surface layer and fractional sea ice are employed as with previous Polar WRF experiments. Due to its strong seasonal dependence [*Perovich et al.*, 2002, 2007], sea ice albedo is allowed to vary during the melt season based on dates of snowmelt over sea ice in a similar manner to the study of Polar WRF over the Western Arctic Ocean [*Bromwich et al.*, 2009]. Sea ice albedo is initially set to 0.82 for winter and spring months. In June, the sea ice albedo linearly decreases with time to 0.5, representing a combination of bare ice and melt ponds. Throughout July, sea ice albedo increases from 0.5 representing a mixed surface to 0.65 representing bare ice only as melt ponds become deeper and less reflective. Melt ponds are no longer treated as part of sea ice albedo calculation by the end of July. Rather, melt ponds are treated as open water within the pack ice. The overall increase in the ice fraction albedo is offset by the fact that less area is covered by bare ice resulting in a decrease in total pack ice albedo. Finally, sea ice albedo linearly increases after

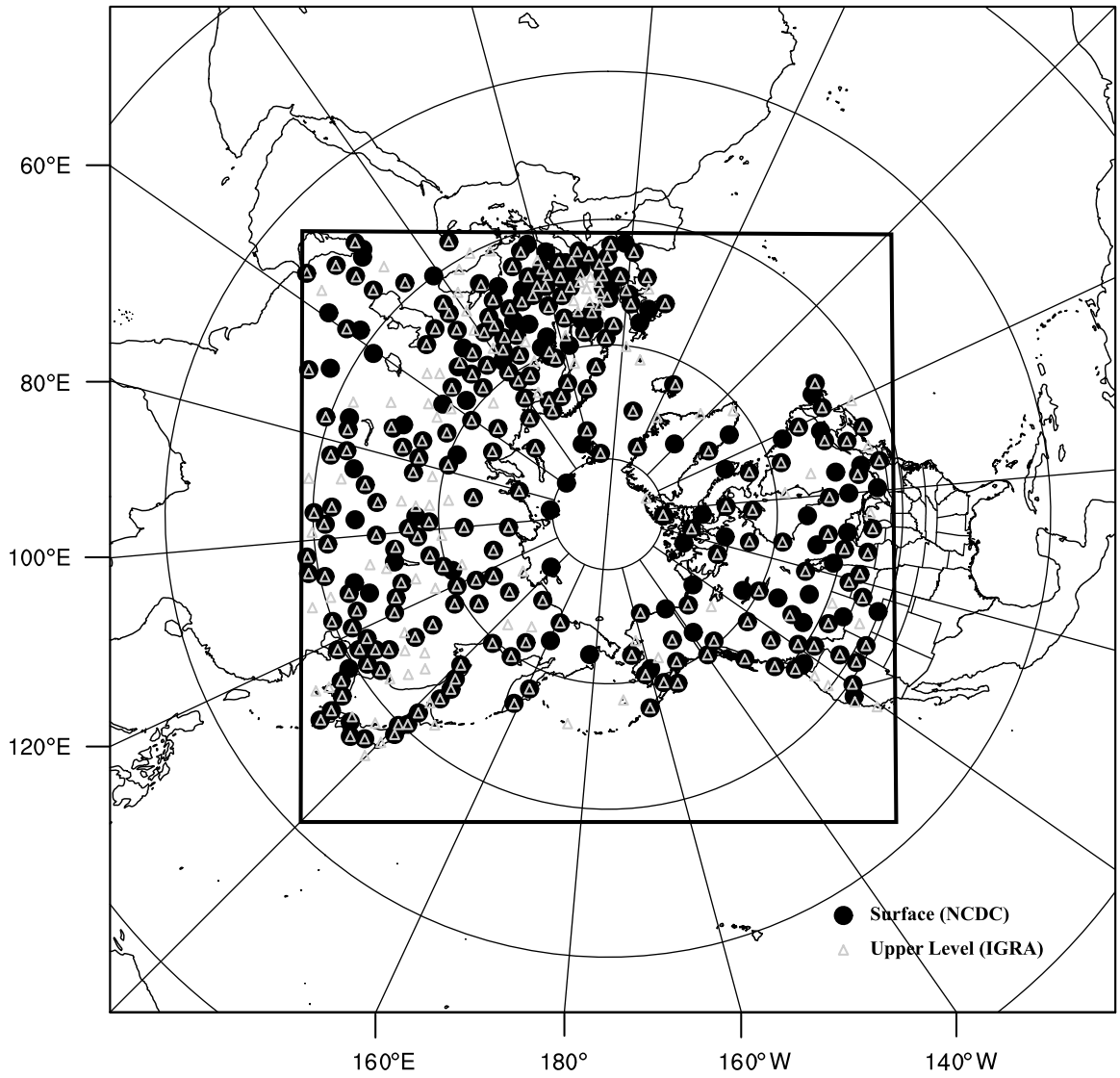

Figure 1. Two-way nested model domain used for Polar WRF simulations. Inner domain consists of 181 × 181 grid points with 60 km horizontal resolution and 39 vertical levels. Included in the inner domain are all surface and upper observations sites used to compare model performance.

August 15, resuming a value of 0.82 by September 1. This process has been extended to 16 sea ice zones within the model domain.

3. Model Domain and Input Data

[10] The domain for this study is consistent with the ASR domain including most of the Northern Hemisphere. The domain is a two-way nested domain centered on the North Pole, with the inner domain extending 10,800 km in the west-east and south-north directions on a 60 km horizontal grid (Figure 1). The two-way runs allow both the inner and outer domains to be run simultaneously, where the coarser outer domain gives boundary conditions to the inner domain and the finer inner domain provides information back to the outer domain. While higher resolution simulations will be conducted with Polar WRF for ASR, 60 km resolution allows for a meaningful broad scale evaluation of Polar WRF behavior on the expansive ASR domain. Likewise, 60 km resolution maintains reasonable tractability and resource management. The inner domain boundaries are located inside the highest terrain of the Tibetan Plateau, include a large portion of the North Pacific and North Atlantic storm tracks, and encompass the Arctic river drainage basins.

[11] The lateral boundary conditions are specified by the *National Center for Atmospheric Research* [1999] Final global gridded analysis archive, a 1° × 1° global grid updated every six hours. Sea surface temperatures are provided by the NCEP 0.5° RTG_SST Analysis [*Gemmill et al.*, 2007]. The sea ice coverage is supplied by the Bootstrap Sea Ice Concentrations from the Defense Meteorological Satellite Program's (DMSP) Special Sensor Microwave/Imager (SSM/I) [*Comiso*, 1999] with 25 km resolution. SSM/I has been used effectively to identify varying ice

types [*Shokr et al.*, 2008] and track seasonal and interannual variability of lake ice cover in the Aral Sea [*Kouraev et al.*, 2009]. Daily sea surface temperature and sea ice concentration are linearly interpolated to six hour inputs based on the difference between two consecutive days.

4. Validation Data and Methods

[12] The surface analysis compares model results to observations from the National Climatic Data Center (NCDC) observations for 2 m temperature, 2 m dewpoint, surface pressure, mean sea level pressure, 10 m wind speed, 10 m wind direction, as well as 10 m wind components. Station locations within the Polar WRF inner domain have been divided regionally along 60°N, with polar stations identified as those lying north of this latitude (upper level analysis as well). Several NCDC stations are located directly on the coast in topographic areas difficult to resolve at 60 km resolution. For the surface evaluation therefore, additional analysis is conducted for stations north of 60°N and at least 100 km away from the coast (polar NC). This allows for a meaningful discussion of model behavior on Arctic land in areas of open terrain. Biases, root mean squared differences (RMSD), and correlation coefficients for all variables are calculated on annual, seasonal, and monthly time scales for each station and means are calculated for each region. A diurnal cycle analysis for selected observations is included to analyze this important aspect of summer model behavior. Although 78% of model surface elevations are within 200 m of NCDC elevations, 2 m temperature and 2 m dewpoint results from model simulations are adjusted to the NCDC station height using the environmental lapse rate of 6.5 K km^{-1}. Likewise, model surface pressure is corrected hypsometrically to NCDC elevations where the temperature is set to the model 2 m temperature at each observation time.

[13] Upper air analysis is conducted using observations from the Integrated Global Radiosonde Archive (IGRA) sounding-derived data set which includes temperature, geopotential height, relative humidity, wind speed, zonal wind component, and meridional wind component observations [*Durre and Yin*, 2008]. Analysis is performed on the following levels: 1000 hPa, 850 hPa, 700 hPa, 500 hPa, 300 hPa, 200 hPa, and 100 hPa, where models results are interpolated to the observed pressure levels. Discussion will focus on radiosonde observations at 850 hPa and above, with 1000 hPa level included only where it has been cross checked with surface results. Likewise, stations included in the analysis must report at least 50% of the monthly radiosonde observations at all pressure levels. Annual and seasonal mean biases, RMSDs, and correlation coefficients for all variables for each level are calculated and regionally averaged. Vertical profiles of biases, RMSDs, and correlation coefficients demonstrating model differences throughout the troposphere are provided, and focus is given to seasonal vertical profiles of polar region temperature and horizontal wind speed in order to provide clarity to the evaluation of model performance in the Arctic. Figure 1 also shows the surface and upper level locations used for Polar WRF comparisons.

[14] Last, the ERA-Interim Reanalysis [*Simmons et al.*, 2006] is used for comparison of annual mean 2 m temperature field as predicted by Polar WRF. ERA-Interim uses a 4D-Var system to merge short-term model forecasts with conventional and satellite observations from 1989 to the present [*Dee and Uppala*, 2009]. ERA-Interim has been shown to perform well in modeling near-surface temperatures over Ireland [*Mooney et al.*, 2010] and in depicting tropospheric temperatures over the Arctic [*Dee and Uppala*, 2009]. Here, the output from ERA-Interim is on a 1.5° × 1.5° latitude/longitude grid and has been projected onto the Polar WRF domain without interpolation in order to provide a qualitative spatial analysis of near surface air temperature and evaporation.

5. Surface Variable Evaluation

[15] Polar WRF and ERA-Interim annual mean 2 m temperatures over land are shown in Figure 2. At 60 km resolution, Polar WRF provides a higher degree of detail across the domain, especially in regions of higher elevation. Examining the extremes, the coldest annual simulated mean surface air temperatures are found just north of the highest elevations over the Greenland ice sheet, with annual mean temperatures ranging from −25°C to −35°C. Spatially, this agrees well with previous mesoscale modeling studies of Greenland using Polar MM5 [*Cassano et al.*, 2001] as well as ERA-Interim. The warmest temperatures in the domain are found in the Persian Gulf region and deserts of Eurasia, with annual mean temperatures exceeding 15°C.

[16] Table 1 summarizes the results of the surface analysis with NCDC and Figure 3 shows individual location results. Two meter temperature biases for the whole domain are generally cold, with an annual mean bias of −0.8°C in the midlatitudes and −1.3°C for the polar region (Figure 3a). The midlatitude region reflects a high degree of skill with an annual mean correlation of 0.84. The correlations are slightly lower in some regions of higher terrain and along coasts, especially in western North America. Many locations in the polar region have correlations ranging from 0.70 to 0.89, with a couple of stations showing correlations less than 0.60. These less skilled stations are located on the coast along the periphery of the Arctic Ocean. However, the annual mean correlation for the polar region when only NC stations are included increases from 0.76 to 0.81.

[17] To explore the seasonal differences, Figure 4 shows the monthly mean biases, RMSDs, and correlation coefficients of 2 m temperature for all months for both the midlatitude and polar regions. Likewise, monthly correlations are plotted for polar (NC) stations. The difference between winter and summer biases in the polar region is larger than the midlatitude region. In the polar region the biases are especially negative in the winter and slightly positive in June and July. July and August correlation coefficients are markedly improved for noncoastal polar stations (0.74/0.83, 0.75/0.85, respectively). Unlike winter conditions when sea ice results in little temperature difference between land and ocean, difficulty arises in summer due to the inability to accurately choose a model grid point location representative of the coastal station and its land surface. The midlatitude biases and correlations change little throughout the year.

[18] Evidence presented here suggests Polar WRF has a cold bias throughout most of the domain compared to both ERA-Interim and NCDC surface observations. First, there is evidence indicating ERA-Interim global mean tropospheric

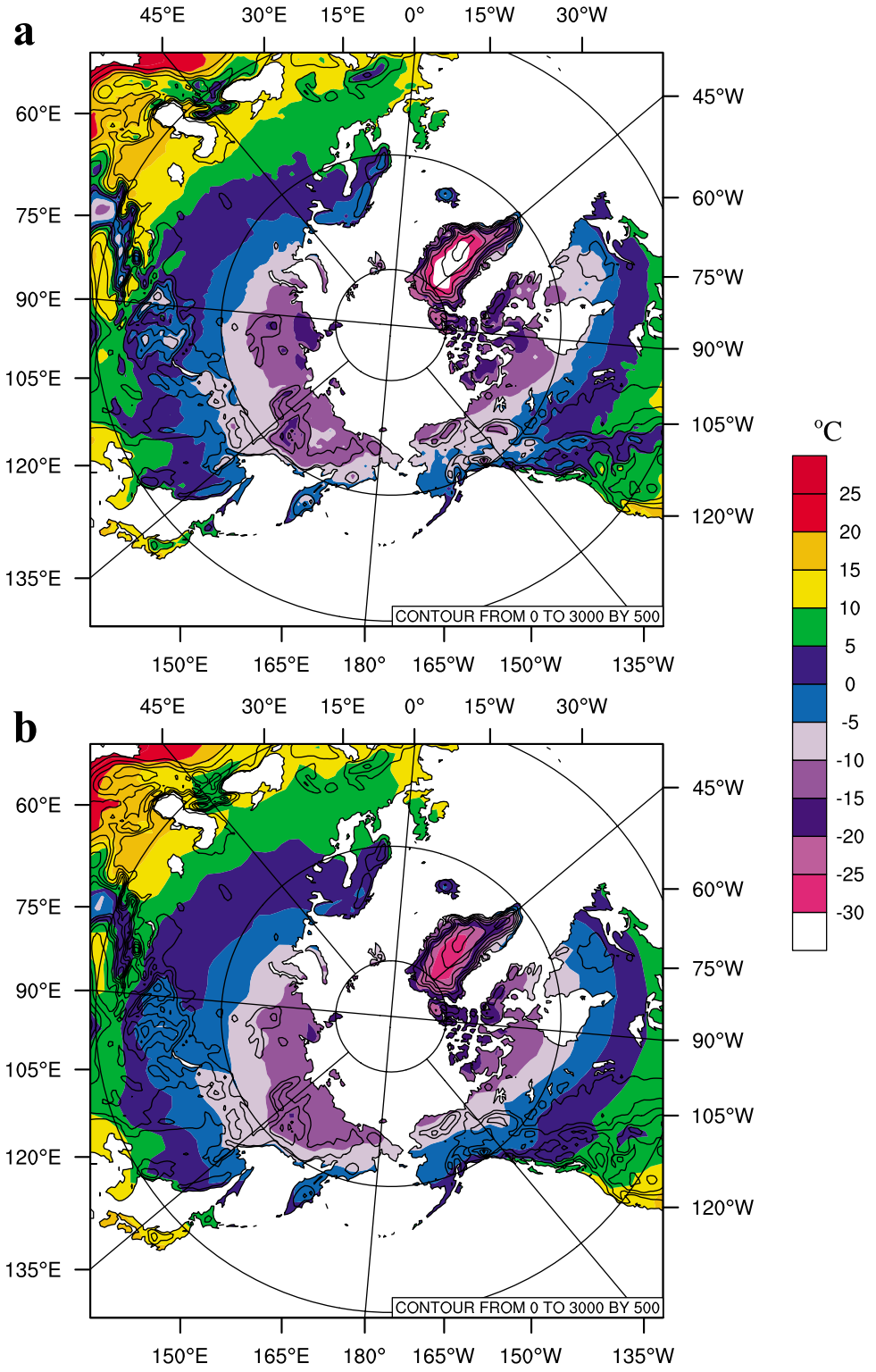

Figure 2. Annual mean 2 m temperatures (°C) over land for (a) Polar WRF and (b) ERA-Interim. ERA-Interim data have not been regridded to Polar WRF resolution.

temperatures are warmer when compared to other reanalyses (ERA-40 and JRA-25) [*Dee and Uppala*, 2008]. Second, earlier Polar WRF studies (with WRF versions prior to 3.1) indicate Polar WRF had a positive bias in the near surface temperatures when compared to selected surface observations. A cold bias has been reported with the Noah LSM beginning with WRF version 3.1 (K. Manning, personal communication, 2011), the cause of which is yet to be determined. This is likely to be the cause of the cold bias found here.

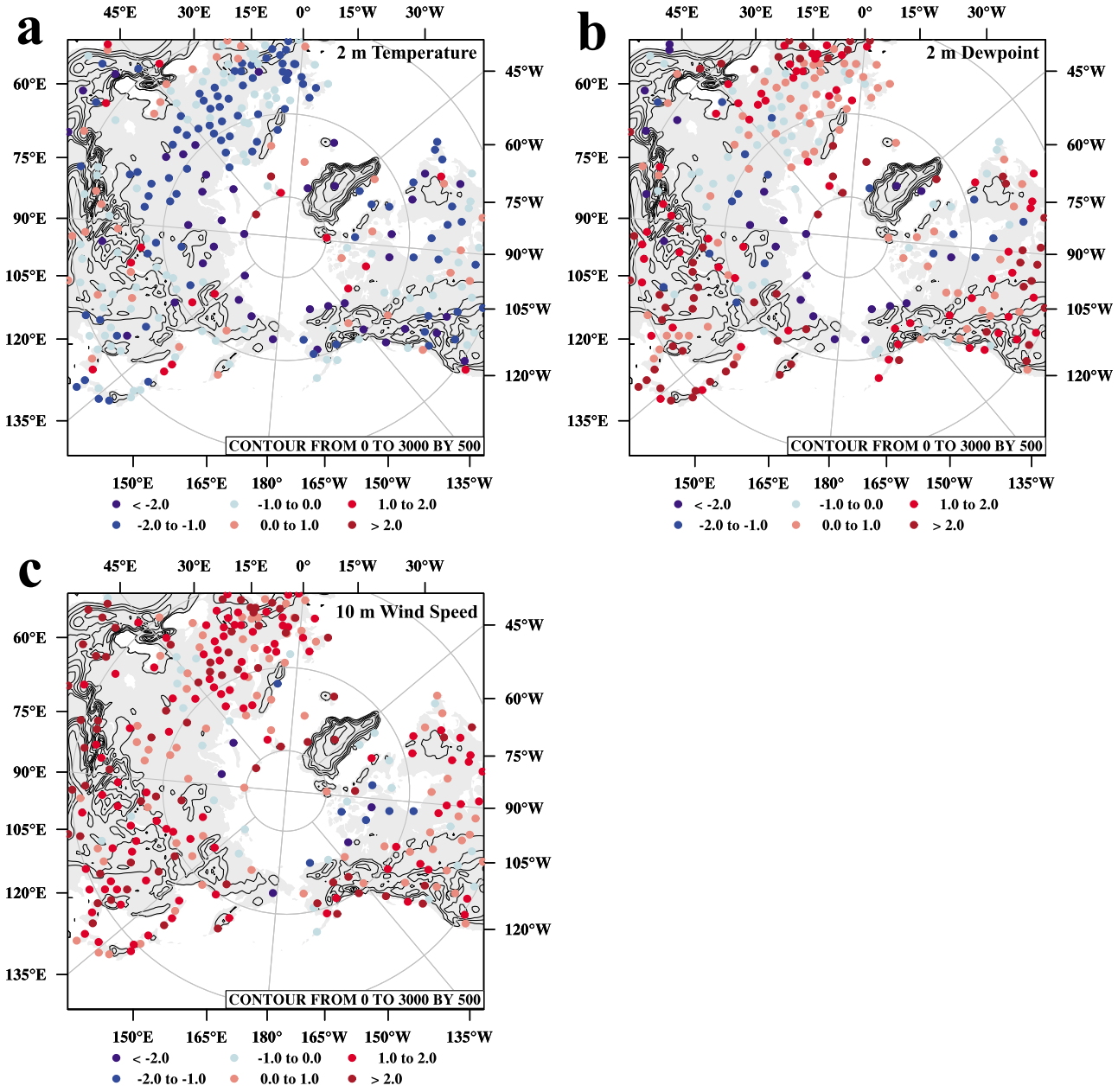

Figure 3. Annual mean biases compared to NCDC surface observations over land for (a) 2 m temperature (°C), (b) 2 m dewpoint temperature (°C), and (c) 10 m wind speed (m s^{-1}). Terrain elevation is contoured from 0 m to 3000 m in 500 m increments.

[19] Unlike annual mean 2 m temperatures which are generally cold everywhere, annual mean 2 m dewpoint temperature biases vary between regions (Figure 3b). The midlatitudes show positive biases while many polar region stations indicate negative biases. Seasonally, 2 m dewpoint temperature biases in the midlatitudes are positive throughout the entire year despite negative 2 m temperature biases, and correlations average 0.73 (Figure 5a). Many locations in Europe for example, show annual mean biases of up to +2°C, especially in Western Europe where the influence of the Atlantic Ocean is greatest. An examination of the 10 m zonal and meridional wind components reveals a negative bias in both components for this region. This indicates the higher 2 m dewpoint temperatures are not the result of water vapor transport from moisture sources.

[20] Instead, increased evaporation from the surface seems the most likely cause, supported by high relative humidity throughout the lower troposphere (Section 6) and excessive precipitation (subsequent paper). A comparison of Polar WRF and ERA-Interim 2 m dewpoint temperatures to NCDC observations for the month of July reveals the biases are larger for Polar WRF than ERA-Interim biases that are near zero (not shown). Figure 6 shows Polar WRF and ERA-Interim total evaporation over land for July 2007.

Table 1. Annual Surface Means[a]

	Bias	Minimum	Maximum	RMSD	Correlation	Obs
			2 m Temperature (°C)			
Midlatitude	−0.8	−4.5	3.7	3.3	0.84	219
Polar	−1.3	−7.0	5.9	4.4	0.76	64
Polar (NC)	−1.6	−5.8	3.2	4.5	0.81	29
			2 m Dewpoint (°C)			
Midlatitude	1.0	−6.1	6.6	3.6	0.73	217
Polar	−0.4	−7.2	6.5	4.4	0.71	66
Polar (NC)	−0.5	−6.0	4.6	4.5	0.73	31
			Surface Pressure (hPa)			
Midlatitude	−0.6	−5.0	4.3	2.8	0.94	185
Polar	−1.5	−4.8	5.1	3.3	0.96	54
Polar (NC)	−1.9	−4.7	1.3	3.4	0.96	26
			Sea Level Pressure (hPa)			
Midlatitude	−1.3	−5.9	4.4	3.4	0.93	195
Polar	−2.5	−5.9	1.0	3.8	0.96	59
Polar (NC)	−3.2	−5.8	−0.03	4.3	0.96	25
			10 m Wind Speed (m s^{-1})			
Midlatitude	1.4	−2.0	3.6	2.6	0.52	214
Polar	0.5	−3.3	3.7	2.7	0.52	67
Polar (NC)	1.1	−1.7	3.5	2.3	0.53	31
			10 m U (m s^{-1})			
Midlatitude	−0.2	−5.4	4.9	4.8	0.62	207
Polar	0.1	−7.2	9.3	5.8	0.64	64
Polar (NC)	−0.2	−3.3	2.3	3.9	0.65	28
			10 m V (m s^{-1})			
Midlatitude	0.1	−4.6	4.7	4.6	0.59	208
Polar	0.2	−5.5	6.1	5.7	0.65	62
Polar (NC)	−0.1	−3.3	4.2	4.1	0.65	27

[a]Here midlatitude stations are those south of 60°N and polar stations are those north of 60°N. Polar (NC) are polar stations at least 100 km away from the coast. Obs represent the number of stations included in each region for each variable.

Polar WRF evaporation is calculated by taking the monthly total latent heat flux and dividing by the latent heat of vaporization (assumed to be a constant at 2.5 MJ kg^{-1}). Throughout the midlatitudes, Polar WRF demonstrates higher monthly total evaporation than ERA-Interim, consistent with higher 2 m dewpoint temperatures. Even some areas of the Arctic (i.e., Siberia and Alaska) reflect higher evaporation totals for July in Polar WRF than ERA-Interim. With excess evaporation indicated by the model in the midlatitudes, solar radiation reaching the surface in these areas is being used to evaporate moisture from the surface instead of warming the near surface air temperature. Therefore, the cold 2 m temperature biases in these regions are also consistent with higher evaporation.

[21] Several polar stations have large negative 2 m dewpoint temperature biases (Figure 3b), which are largely following the behavior of 2 m temperatures (Figure 3a). Spring and summer months demonstrate positive dewpoint biases during a time of increased evaporation (Figures 5b and 6). For the remaining seasons, negative 2 m dewpoint temperature biases exist, with slightly lower correlations than the midlatitudes (0.71/0.73 for NC).

[22] Surface pressure and sea level pressure (both included to capture a higher amount of available stations in the domain) primarily reflect negative annual mean biases, ranging from −3.2 hPa to −0.6 hPa for all regions considered. While the greatest negative biases in surface pressure appear to be confined to the Eurasian continent, negative sea level pressure biases can also be found in northwest North America. Polar WRF demonstrates a high level of skill in predicting the overall synoptic pressure environment. Few locations show correlations less than 0.90 and these are restricted to higher elevations throughout Asia and Europe, where elevations exceed 3000 m. Likewise, high correlations are found throughout all months of the simulation, with little variation in the biases (not shown).

[23] Finally, annual mean 10 m wind speed biases are less than 2 m s^{-1} with Polar WRF demonstrating a small bias in the polar region (0.5 m s^{-1}). Many locations throughout the domain reflect positive 10 m wind speed biases. However, biases for the zonal and meridional wind components of the 10 m wind speed are smaller. Thus, no one component contributes primarily to the overall positive 10 m wind speed biases as both the zonal and meridional components vary greatly by location. The annual mean 10 m wind speed correlations are by far the lowest correlations for the surface variables analyzed. The likely reason for both the poor correlations and the strong wind speeds is the relatively coarse model resolution and the resulting inability to accurately predict local wind effects (at 60 km resolution). Also, 60 km resolution effectively smoothes the terrain leading to an overprediction in the 10 m wind speed. With a horizontal model resolution of 10 km and the addition of data assimilation, ASR should improve the predictive skill of 10 m wind speed. Despite the inability to account for local effects on wind speed, the 10 m wind speed correlations are reasonably captured across Western and Northern Europe and in areas of flat terrain.

6. Diurnal Cycles of Surface Variables

[24] The average diurnal cycles of 2 m temperature, 2 m dewpoint temperature, and 10 m wind speed for January and July 2007 have been calculated using the same method employed by *Cassano et al.* [2001], namely finding the monthly averaged departure from the daily mean for each time (3 hourly NCDC observations or Polar WRF output). Regional averages have been calculated in order to synthesize the behavior over the entire domain. Figure 7 shows the domain divided longitudinally into 8 regions beginning with ±22.5° around 0° and gives the number of stations included in the midlatitude and polar regions. With some discrepancy, these regions reflect similar topography and weather patterns.

[25] As expected, the diurnal cycles for all 8 regions are smallest in January. As the solar radiation decreases across the Northern Hemisphere to its winter minimum, there is a smaller diurnal cycle of temperature. Also, many regions in the Northern Hemisphere experience cloudier conditions during winter which also contribute to decreasing the difference between maximum and minimum temperatures. Therefore analysis will focus on July 2007 diurnal cycles.

[26] First, of all 8 regions the smallest diurnal temperature range in the midlatitudes (Polar WRF and observations) is found in region 4 (not shown). This is not surprising, as many of the stations within this region are highly influenced

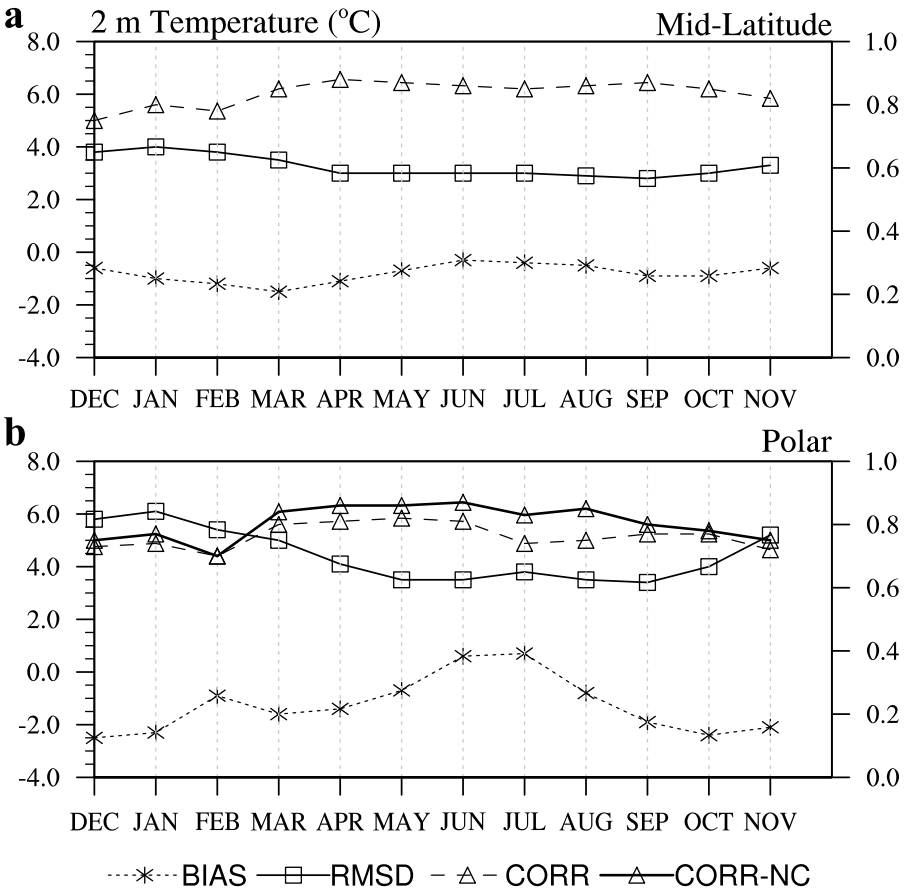

Figure 4. Monthly mean 2 m temperature biases, RMSDs, and correlation coefficients for (a) midlatitude region and (b) polar region. Correlation coefficients are also provided for the noncoastal polar region stations at least 100 km away from the coast (NC). The left-hand scale applies to bias and RMSD while the scale on the right is for correlation.

by their maritime locations near the North Atlantic Ocean. For this region, the differences in diurnal cycles between model and observed 2 m temperature, 2 m dewpoint temperature, and 10 m wind speed are small and well contained within the standard error.

[27] For the remaining regions, small variations exist but are well represented by the average diurnal cycle for region 3. This region consists of 23 midlatitude stations and is located in Central Canada and the Northern Great Plains (Figure 7). For 2 m temperatures, the diurnal cycle is reproduced well but exhibits a larger range when compared to observations (Figure 8). In fact, all regions in this analysis show larger model diurnal 2 m temperature ranges. The error bars reveal that largest differences between the model and observations occur from 0900 to 1500 and at night.

[28] The average diurnal cycle of 2 m dewpoint temperature shows nearly zero diurnal variation. Again, the model captures this behavior well with significant differences occurring at the same time as significant differences in the 2 m temperature diurnal cycle. Regions 2 and 5 are greatly influenced by the ocean and have a larger diurnal range in 2 m dewpoint.

[29] Finally, the 10 m wind speed monthly average diurnal cycle shows insignificant differences between the model and observations. However, Figures 8a and 8c demonstrate the model's coupling between near surface temperature and wind is strong. Due to the larger diurnal 2 m temperature range, temperatures rise and fall quicker than the observations. The near surface winds respond to this rapid change as seen in Figure 8c. When static stability is high (at night) the model and observations vary little. However, during the daytime (decreased stability) when vertical mixing is highest, the model and observations differ significantly.

[30] Figure 9 shows the average monthly diurnal cycles for all variables for July 2007 from region 2 north of 60°N. This region has 7 stations of which 5 are noncoastal. Of particular note is the large diurnal 2 m temperature range (greater than the midlatitude cycle), where significant differences between the model and observations occur near the highest and lowest solar angles. *Hines et al.* [2011] show that clouds and radiation are sensitive to the choice of microphysics and boundary layer parameterizations when dealing with areas near the Arctic Ocean, but are not sensitive for areas inland. The result is an underrepresentation of (Arctic) stratus clouds over Arctic land in the summer.

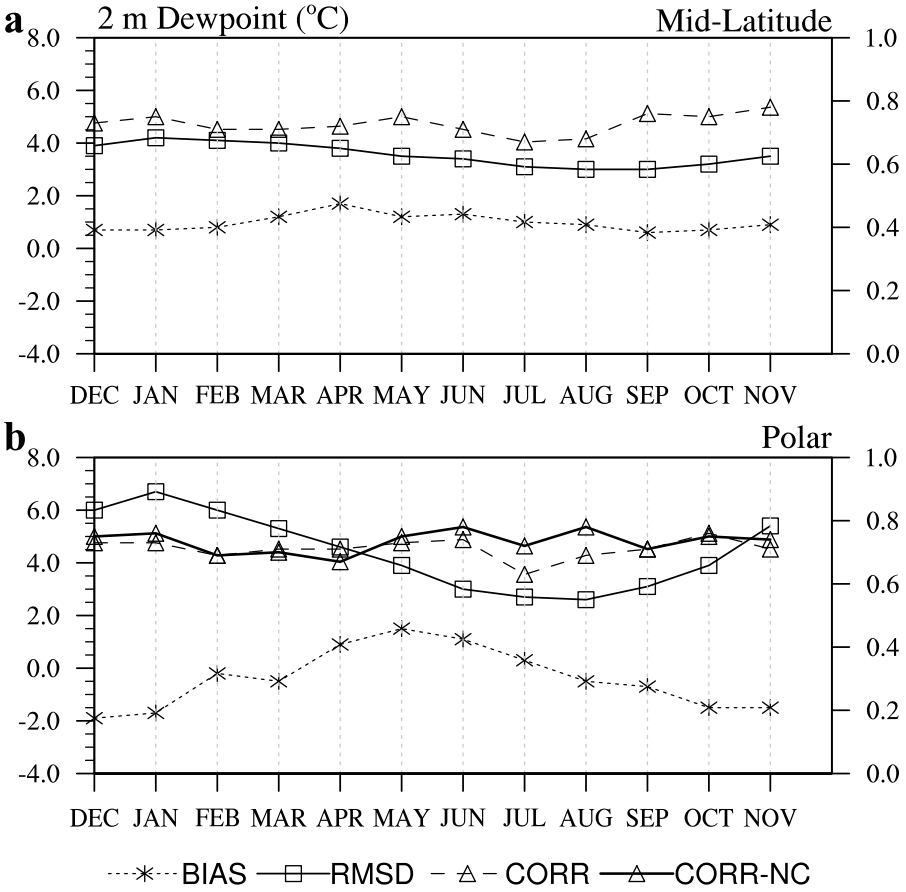

Figure 5. Monthly mean 2 m dewpoint temperature biases, RMSDs, and correlation coefficients for (a) midlatitude region and (b) polar region. Correlation coefficients are also provided for the noncoastal polar region stations at least 100 km away from the coast (NC). The left-hand scale applies to bias and RMSD while the scale on the right is for correlation.

This causes an overly amplified diurnal cycle (such as presented here) due to increased incident shortwave radiation in the model during the day and too few clouds radiating heat toward the surface during the night.

[31] Overall, the average observed diurnal cycle of 2 m dewpoint temperature in the polar region is nearly zero, with the greatest differences in amplitude between Polar WRF and observations occurring at 1800 and 0300 local time. It has been shown that evaporation is high in the model during July 2007 (Figure 6). Combined with higher than observed 2 m temperature in the model at 1800 (Figure 9a), increased evaporation leads to more moisture near the surface. Lower than observed 10 m wind speed at this time corresponds to decreased vertical mixing of the near surface moisture (Figure 9c). Higher model temperatures also occur from 0600 to 1500 local time, but the dewpoint temperature cycle is only slightly higher than the observed. The model 10 m wind speeds are greater at this time which leads to more vertical mixing of excess moisture.

[32] Evidence presented here from both the midlatitude and polar region indicate that the model well represents the average diurnal cycles for 2 m temperature, 2 m dewpoint temperature, and 10 m wind speed. The larger diurnal 2 m temperature ranges affect both the dewpoint and wind speed cycles, resulting in increased vertical mixing in the model during the day as well as higher evaporation near the surface and higher dewpoint temperatures when the winds are light.

7. Annual Means of Upper Air Variables

[33] The annual means of biases, RMSDs, and correlation coefficients for temperature, geopotential height, relative humidity, and wind speed at the previously mentioned pressure levels are calculated and plotted in Figure 10. The annual mean temperature bias is generally small, ±1°C throughout the entire column for both the midlatitude and polar regions (Figure 10a). Both regions show a negative bias near the surface, with a positive bias occurring at 300 hPa (0.2 for midlatitude region and 0.6 for the polar region). RMSD values range from 1°C to 2°C, and reflect typical Polar WRF temperature errors throughout all the levels with respect to observations (except near the surface in the polar region). Correlation coefficients for all levels at or above 850 hPa are high and range from 0.85 to 0.95, with a small decrease in skill near 300 hPa and 100 hPa. Vertical profiles for winter and summer are also analyzed (not shown). Seasonally, temperature biases are negative in all seasons near the surface and demonstrate the largest positive bias at 300 hPa.

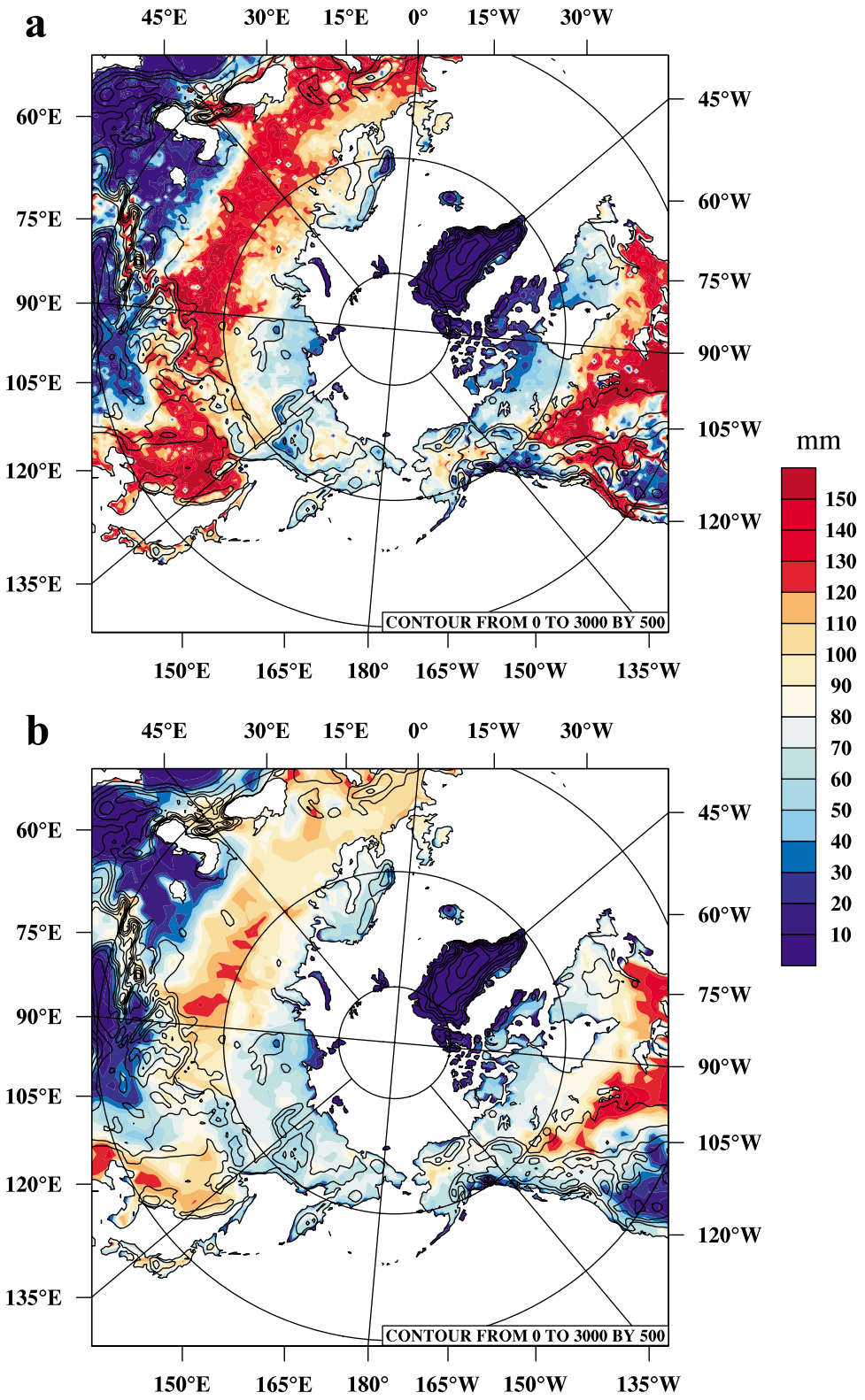

Figure 6. July 2007 total evaporation (mm) over land for (a) Polar WRF and (b) ERA-Interim. ERA-Interim data have not been regridded to Polar WRF resolution. Terrain elevation is contoured from 0 m to 3000 m in 500 m increments.

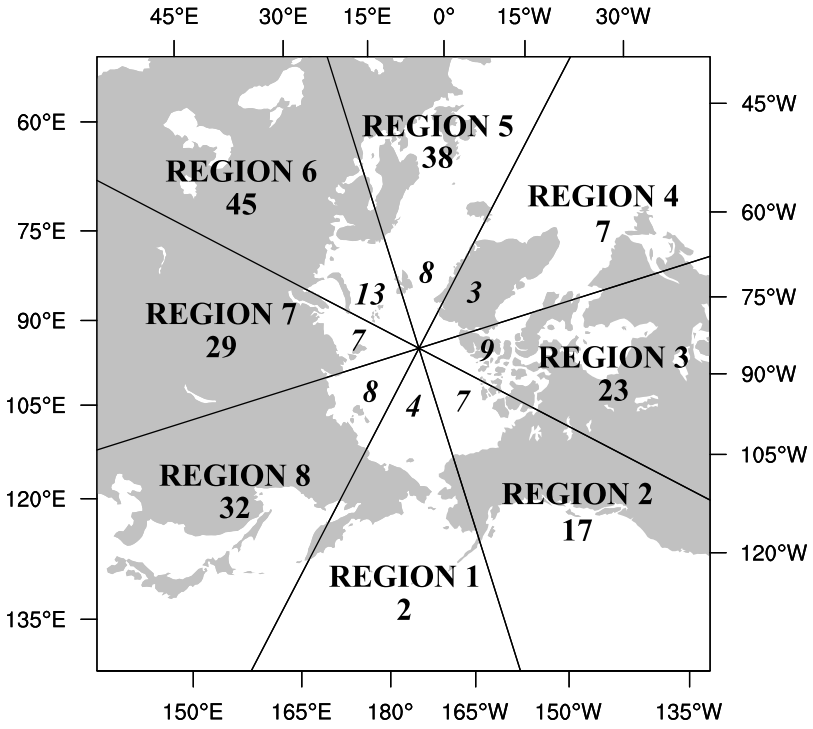

Figure 7. Polar WRF domain divided into eight regions every 45° longitude for diurnal cycle analysis. The number of midlatitude stations is boldfaced, and the number of polar region stations is italicized.

[34] Figure 10b shows the annual mean biases, RMSDs, and correlations for geopotential height plotted to 200 hPa. Only a few stations reported geopotential height at 100 hPa thus this level is excluded from the analysis. The bias is negative throughout most of the atmosphere for both regions, except near and above 300 hPa. Excluding levels near the top of the modeled atmosphere, biases range from −6 m to +30 m in the midlatitudes and from −11 m to +40 m in the polar region. The negative bias in the lower levels is present throughout all seasons, with the least negative biases seen in the summer months. RMSD values range from 20 m to as much as 50 m near 200 hPa. However, geopotential height correlations depict the highest skill of any of the upper level variables, ranging from 0.90 to 0.98 throughout the entire column.

[35] Humidity measurements are the most challenging of upper level variables to accurately observe, especially during cold conditions, making relative humidity difficult to verify [*Elliott and Gaffen*, 1991; *Miloshevich et al.*, 2001].Therefore, midlatitude comparisons are truncated at 300 hPa while polar region comparisons are limited to 500 hPa and below due to observational limitations. Figure 10c shows on most pressure levels, relative humidity biases range from 1 to 5% in the midlatitudes, with smaller biases in the polar region. This corresponds well with the overall positive 2 m dewpoint temperature biases discussed in section 5. RMSD values depict errors of 15–20% for levels at or below 500 hPa. Again, the correlation coefficients reflect overall lower skill, ranging from 0.55 to 0.65 at 850 hPa, 700 hPa, and 500 hPa.

[36] For wind speed (Figure 10d), the model tends to be stronger than observations near the surface where the effects of terrain smoothing are greatest, with weaker than observed wind speeds near the top of the model atmosphere. The exception to this occurs near 200 hPa in the polar region. Overall, biases range from −1.1 m s^{-1} in the upper levels to +1.9 m s^{-1} near the surface. In addition, the 1000 hPa wind speed biases are comparable to the near surface biases from the NCDC data set in section 5. The largest positive biases are in the midlatitudes, and wind speeds are overpredicted in the zonal component. This infers increased westerly winds in the midlatitudes, which matches well with a regional plot showing individual station biases of the zonal wind component at 850 hPa (not shown). While correlations near the surface are still low (~0.50), wind speed correlations improve dramatically at pressure levels at or above 850 hPa (0.69–0.92).

[37] A closer inspection of the upper level temperature biases throughout the domain reveals some regional differences (Figure 11). A slightly negative bias (−0.2°C) exists at 850 hPa in the polar region contributed primarily by Greenland station biases. However, at 300 hPa nearly all stations in the domain reflect a warm bias. This bias extends into the midlatitude region, across northern North America and Alaska. While the biases are small (0–2°C), Polar WRF tropopause heights are lower than documented heights over the Arctic (not shown) and is likely the cause of the warm biases [*Zängl and Hoinka*, 2001].

8. Arctic Vertical Profiles of Temperature and Horizontal Wind Speed

[38] In order to describe the Polar WRF upper air performance in the polar region in more detail, monthly mean vertical profiles of temperature and horizontal wind speed are

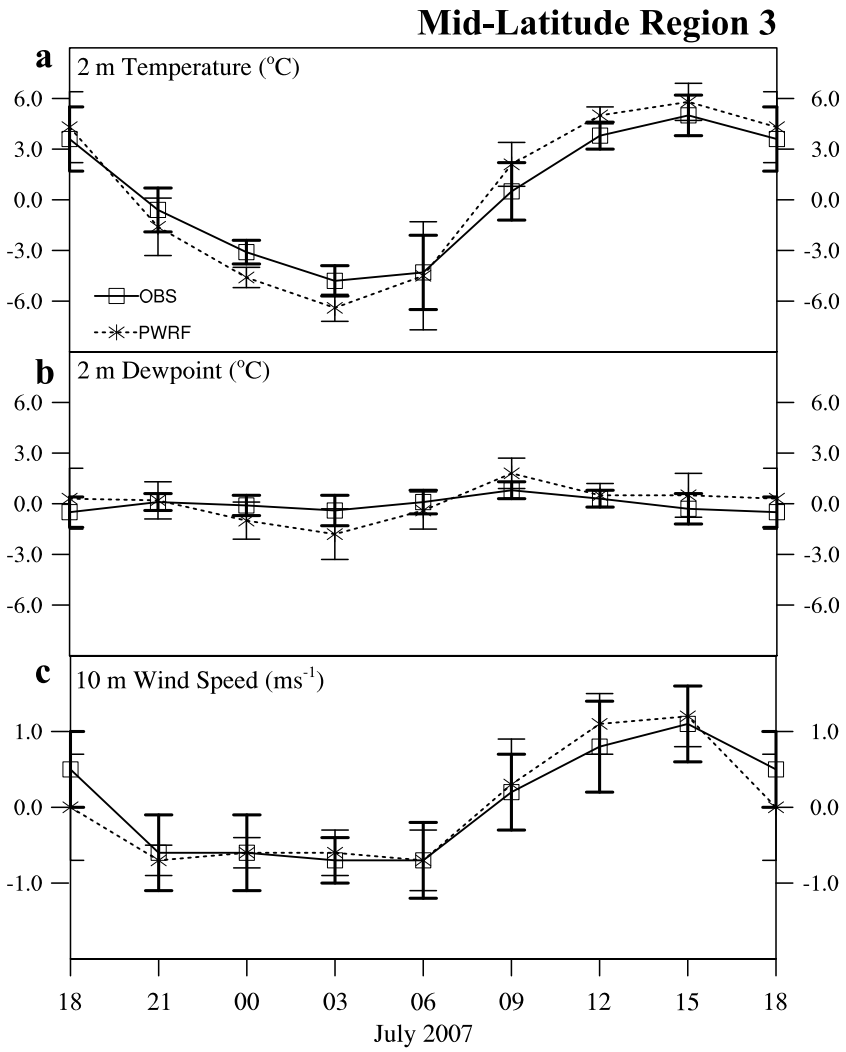

Figure 8. Average monthly diurnal cycles (Region 3) for July 2007 in the midlatitude region. Polar WRF (dashed line) and observations (solid line). The *x* axis is in local time for central meridian of Region 3 (UTC – 6 h). (a) The 2 m temperature (°C), (b) 2 m dewpoint temperature (°C), and (c) 10 m wind speed (m s^{-1}). The standard error is plotted at each observation (model output) time as vertical bars.

calculated. Monthly means are calculated using 0000 UTC and 1200 UTC soundings and match model output times. While the observations only include the 7 major pressure levels, model only profiles consist of all 39 vertical levels described in the model configuration.

[39] Figure 12 shows the monthly mean vertical temperature profiles for 68 polar region stations (dashed line) and the polar region mean (solid line) for January 2007 and July 2007 for both IGRA observations and Polar WRF, along with the means only (Polar WRF dashed and observations solid). Upon initial evaluation, the model appears to represent the temperature observations well throughout the entire column for both months (Figures 12a–12f). For all stations, the modeled and observed temperatures show the largest spread near the surface and near the top. At the surface, the temperature spread in January (~40°C) depicts both the geographical differences among stations included in this analysis along with varying surface characteristics. Likewise, since no direct solar radiation is received at the polar stations until the end of the month, temperature variability near the surface in January is primarily the effect of large synoptic influence on temperature during this time. For July 2007 (Figures 12d and 12e), the Polar WRF modeled temperature profiles match well with observations. Subtle insignificant differences are evident near the surface and above 500 hPa. Although small, Polar WRF temperatures are slightly warmer at levels above 500 hPa, supporting lower than observed tropopause heights. Throughout the middle region of the atmosphere, both observations and Polar WRF show little spread and agree well with one another.

[40] Finally, monthly mean vertical profiles of horizontal wind speed for January 2007 and July 2007 are shown in Figure 13. For both January and July, the overall vertical profile in wind speed is similar between observations and Polar WRF. For January 2007 (Figures 13a–13c), the winds generally increase with height throughout the column, with peaks in modeled wind speed just off the surface, at 300 hPa, and again near the top of the modeled atmosphere. However,

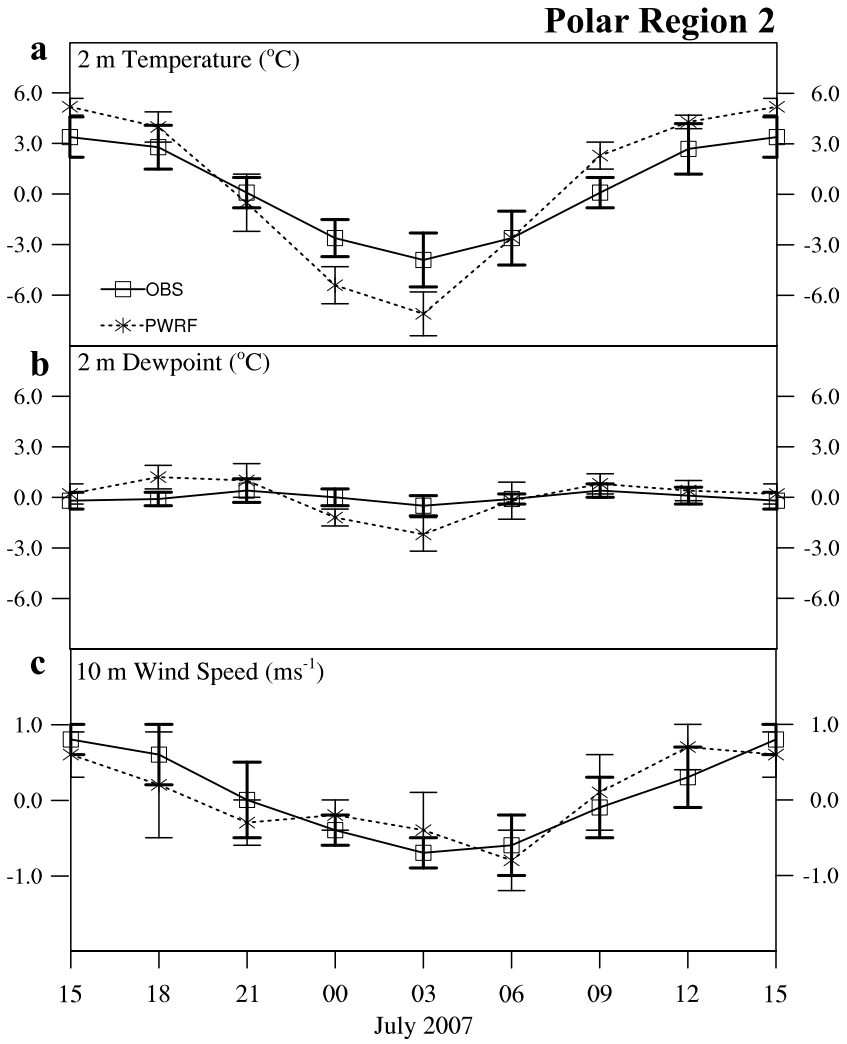

Figure 9. Average monthly diurnal cycles (Region 2) for July 2007 in the polar region. Polar WRF (dashed line) and observations (solid line). The *x* axis is in local time for central meridian of Region 2 (UTC – 9 h). (a) The 2 m temperature (°C), (b) 2 m dewpoint temperature (°C), and (c) 10 m wind speed (m s^{-1}). The standard error is plotted at each observation (model output) time as vertical bars.

the error bars in Figures 13c and 13f indicate that the differences between the model and observed horizontal wind speed profiles are insignificant. Figures 13d–13f show the mean monthly horizontal wind speed vertical profiles for July 2007. The winds are generally weaker in July than during January, and both observations and Polar WRF show a gradual increase in wind speeds with height, with a wind speed maximum occurring around 300 hPa. Unlike the strong winds near the top of the column in winter, the summer plot reflects weaker wind speeds in this region of the stratosphere during this time.

9. Summary and Conclusions

[41] In preparation for ASR, state variables from Polar WRF short-term forecasts during an annual cycle have been examined in this study. Polar WRF has demonstrated to simulate observations of surface and upper air variables well. This is especially true in areas away from complex terrain.

[42] Polar WRF predicted near-surface temperatures agree well spatially with ERA-Interim. Annual mean temperatures from Polar WRF when compared to NCDC station observations are cold throughout most of the domain. However, the biases are small and correlations are high giving confidence that Polar WRF can accurately predict 2 m temperature on an annual cycle. Seasonally, Polar WRF is consistently cold in the midlatitudes while demonstrating a slightly warm bias in the summer months for stations north of 60°N. Not surprisingly, results of the analysis with 2 m dewpoint follow the 2 m temperature patterns in the polar region. However, 2 m dewpoint temperatures show a warm bias in the midlatitudes, the likely result of increased evaporation from the surface.

[43] For sea level and surface pressure, Polar WRF predicted values are the best of all the near-surface variables.

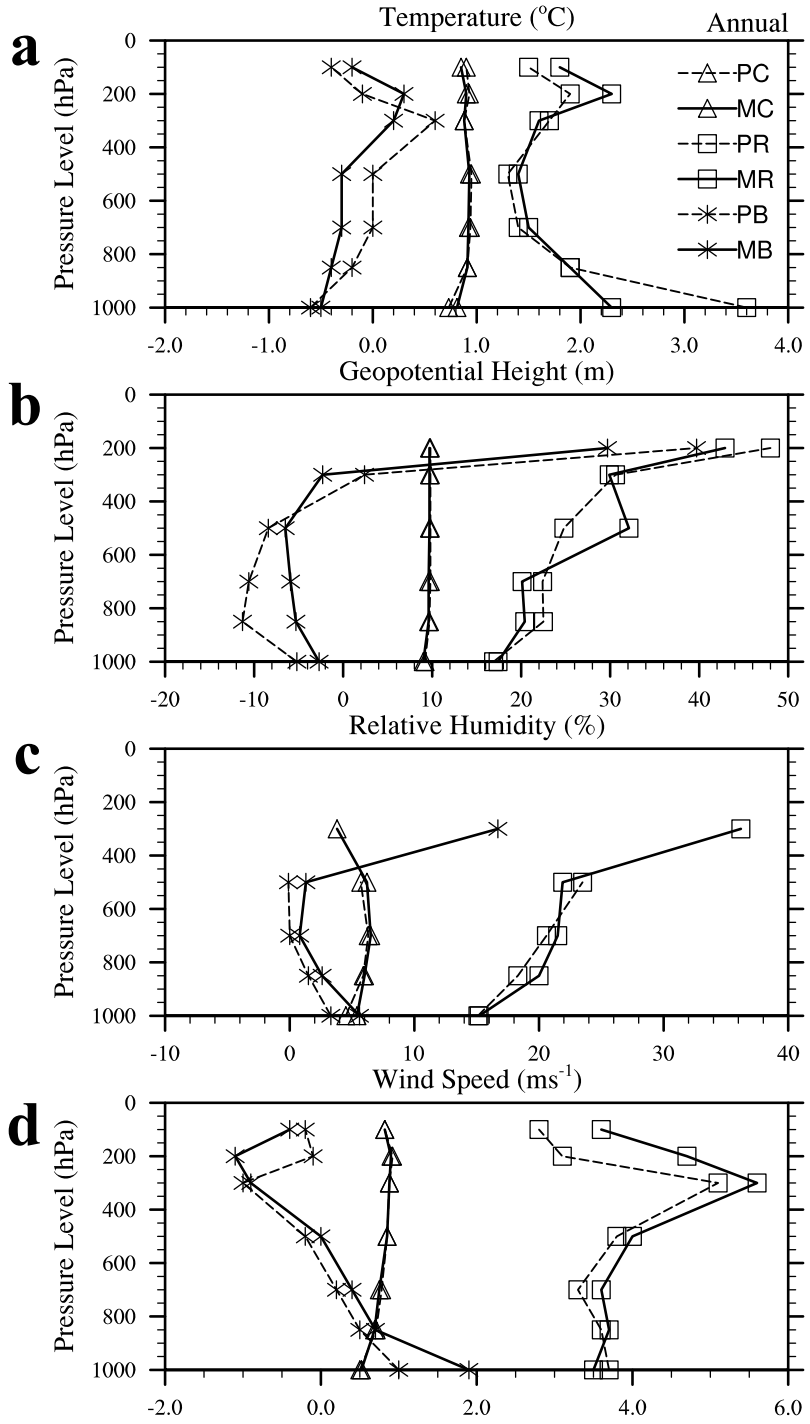

Figure 10. Annual mean biases, RMSDs, and correlation coefficients for midlatitude region (solid lines) and polar regions (dashed lines) for 1000 hPa, 850 hPa, 700 hPa, 500 hPa, 300 hPa, 200 hPa, and 100 hPa. (a) Temperature (°C), (b) geopotential height (m), (c) relative humidity (%), and (d) wind speed (m s^{-1}). MB, midlatitude bias; PB, polar bias; MR, midlatitude RMSD; PR, polar RMSD; MC, midlatitude correlation; PC, polar correlation. Note that correlations for geopotential height and relative humidity are multiplied by 10.

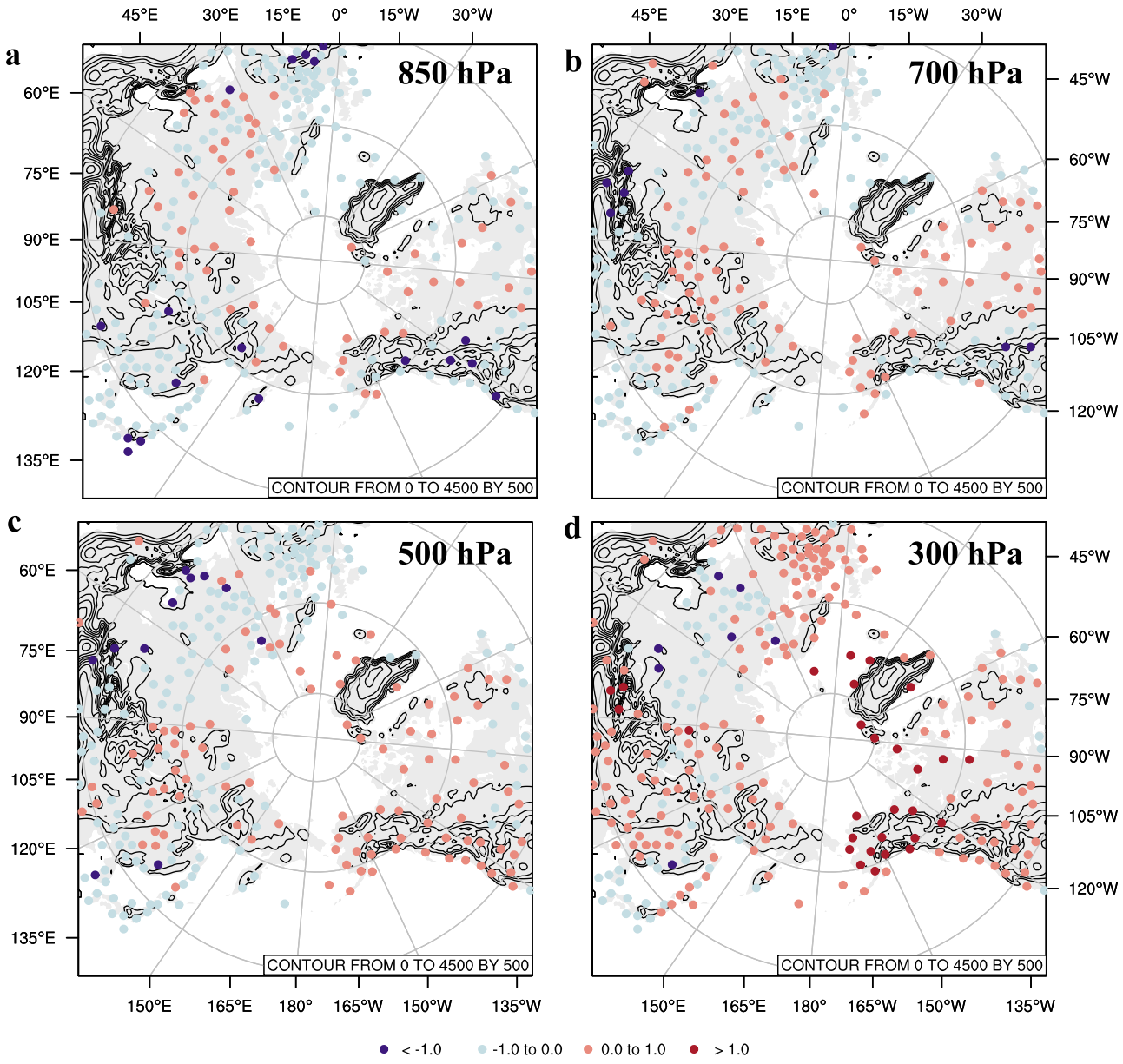

Figure 11. Annual mean temperature biases for all IGRA observations within the Polar WRF domain at (a) 850 hPa, (b) 700 hPa, (c) 500 hPa, and (d) 300 hPa. Terrain heights are contoured, ranging from 0 to 4500 m in 500 m increments.

Correlations for these variables typically range above 0.95 with a slight negative bias throughout the entire year. However, near-surface wind speed is the poorest of all the predicted surface variables. It is believed the coarse model resolution introduces a large amount of error due to inadequate modeling of local wind effects and obstructions.

[44] Further analysis of the diurnal variations in temperature throughout the entire domain reveals that during July, Polar WRF overpredicts temperatures during the day and underpredicts temperatures at night. This also affects the diurnal variations in 10 m wind speed. Differences between the model and observations are small at night under simulated stable conditions. As Polar WRF heats quickly during the morning, the increase in vertical mixing leads to increased surface wind speeds, which is also evident through the diurnal evaluation.

[45] In addition to near-surface variables, it is found that Polar WRF simulated tropospheric temperatures, geopotential heights, and wind speeds improve at pressure levels above the ground surface. Model biases are generally less than 1°C with the largest bias depicted at 300 hPa as a result of lower than observed tropopause heights. However, Polar WRF appears to overpredict the strength of the westerlies, especially in the midlatitudes.

[46] The atmospheric hydrologic cycle will be examined in a follow up investigation using the same simulation. The focus will be on precipitation, clouds, and surface energy budget. Insights from this hydrologic survey along with the

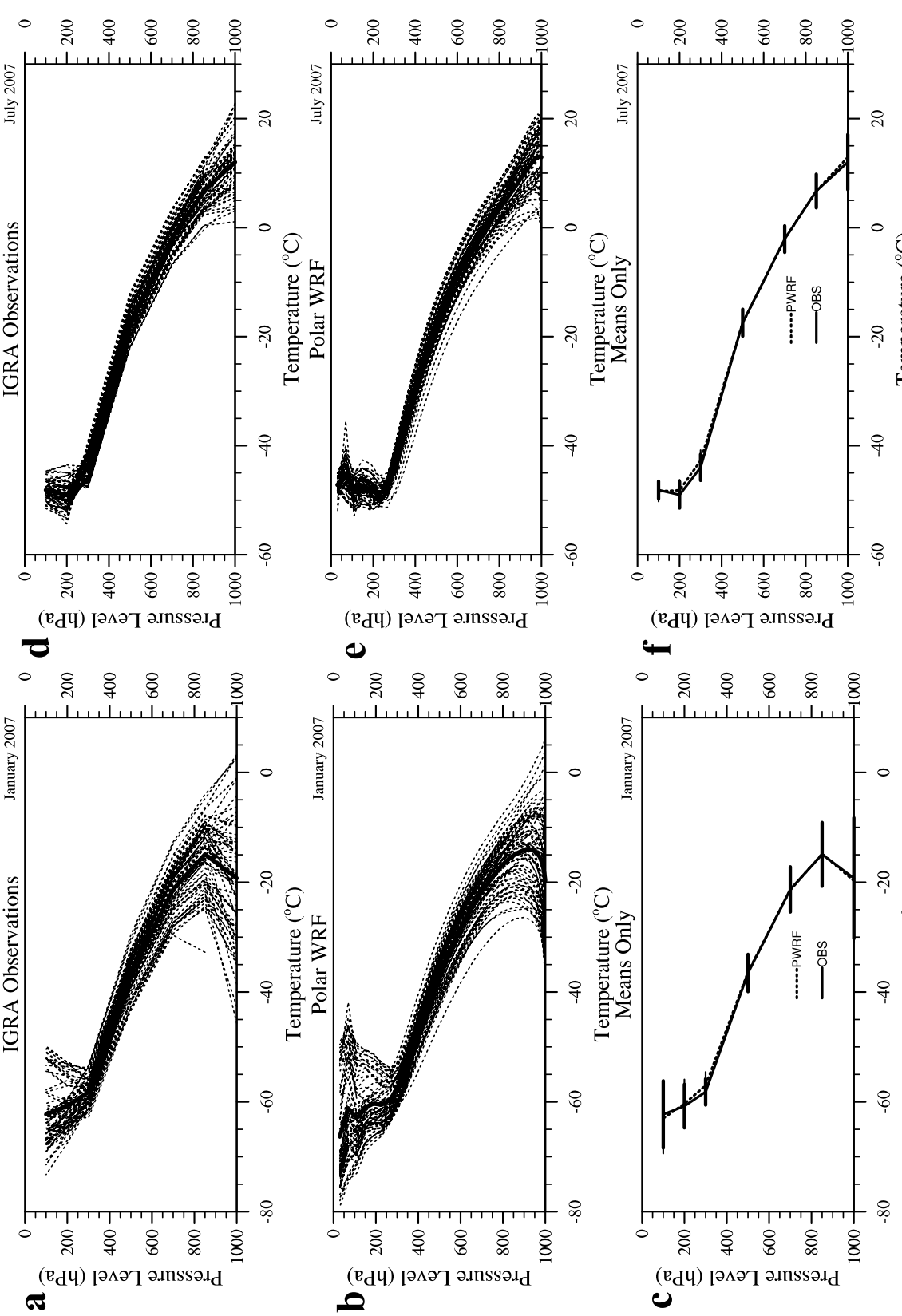

Figure 12. (a–c) January 2007 and (d–f) July 2007 monthly mean vertical temperature profiles (°C) for 68 polar region stations from IGRA (Figures 12a and 12d), Polar WRF (Figures 12b and 12e), and means plotted at observation levels only (Figures 12c and 12f). For Figures 12a, 12b, 12d, and 12e, individual stations are dashed lines and regional mean is solid line. For means only Figures 12c and 12f, Polar WRF mean is dashed line and observation mean is solid line. Thick horizontal bars represent standard error for observations. Thin horizontal bars represent standard error for Polar WRF.

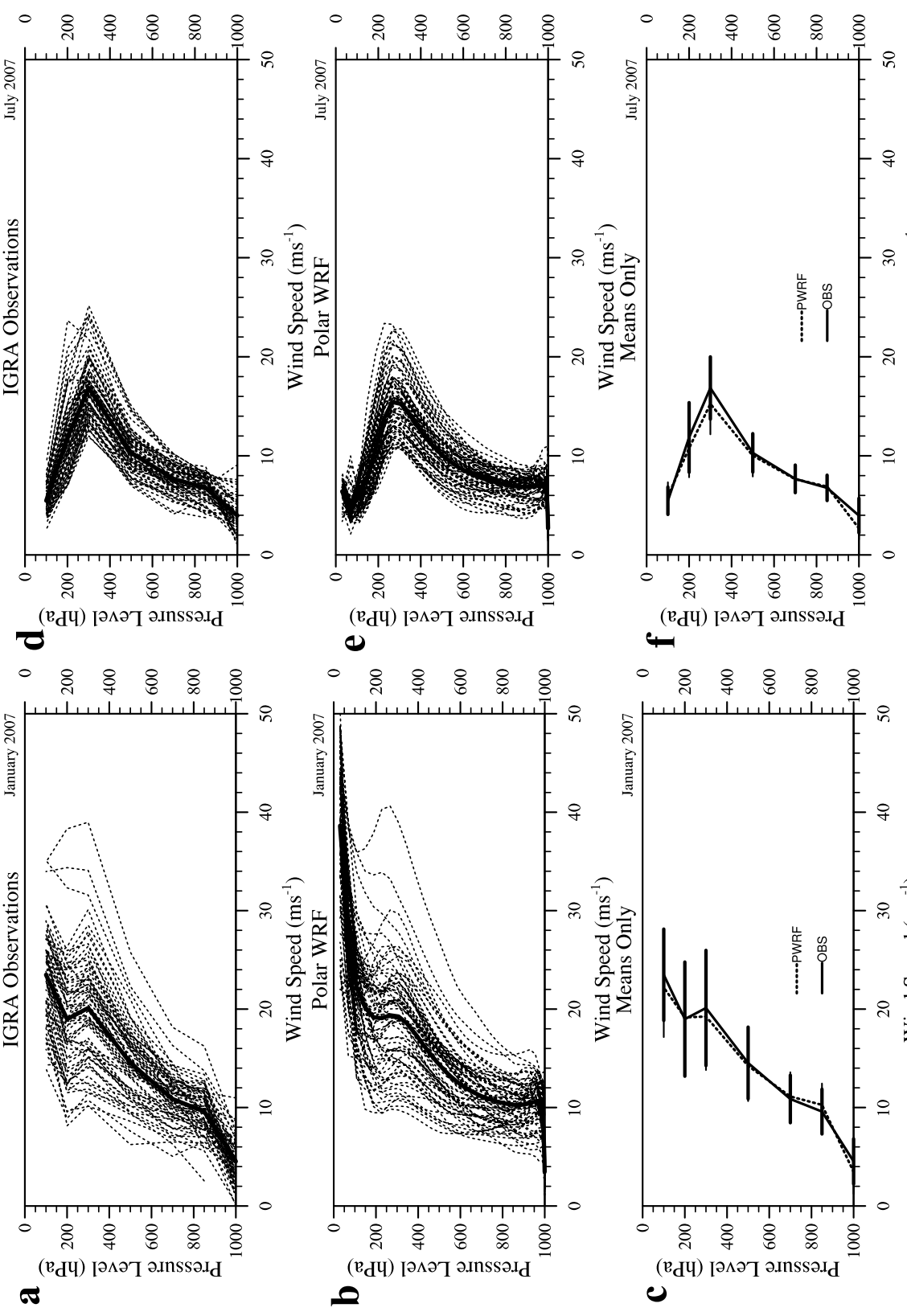

Figure 13. (a–c) January 2007 and (d–f) July 2007 monthly mean vertical distribution of horizontal wind speed profiles (m s^{-1}) for 68 polar region stations IGRA (Figures 13a and 13d), Polar WRF (Figures 13b and 13e), and means plotted at observation levels only (Figures 13c and 13f). For Figures 13a, 13b, 13d, and 13e, individual stations are dashed lines and regional mean is solid line. For means only Figures 13c and 13f, Polar WRF mean is dashed line and observation mean is solid line. Thick horizontal bars represent standard error for observations. Thin horizontal bars represent standard error for Polar WRF.

results presented here will provide a benchmark for Polar WRF's use in ASR.

[47] **Acknowledgments.** This research is supported by NSF IPY grant ARC-0733023 and is contribution 1405 of the Byrd Polar Research Center. The authors would like to thank Francis Otieno and Lesheng Bai for their insightful discussions, Mark Anderson of the University of Nebraska for his sea ice melting onset dates, and Kevin Manning and Jimy Dudhia of the NCAR Earth System Laboratory on their discussion of Noah LSM bias.

References

Arctic Research Consortium of the United States (2005), Study of environmental Arctic change: Plans for implementation during the International Polar Year and beyond, report, 104 pp., Fairbanks, Alaska.

Bromwich, D. H., L.-S. Bai, and G. G. Bjarnson (2005), High-resolution regional climate simulations over Iceland using Polar MM5, *Mon. Weather Rev.*, *133*, 3527–3547, doi:10.1175/MWR3049.1.

Bromwich, D. H., K. M. Hines, and L.-S. Bai (2009), Development and testing of Polar WRF: 2. Arctic Ocean, *J. Geophys. Res.*, *114*, D08122, doi:10.1029/2008JD010300.

Bromwich, D. H., Y.-H. Kuo, M. Serreze, J. Walsh, L.-S. Bai, M. Barlage, K. M. Hines, and A. Slater (2010), Arctic System Reanalysis: Call for community involvement, *Eos Trans. AGU*, *91*(2), 13–14, doi:10.1029/2010EO020001.

Cassano, J. J., J. E. Box, D. H. Bromwich, L. Li, and K. Steffen (2001), Evaluations of Polar MM5 simulations of Greenland's atmospheric circulation, *J. Geophys. Res.*, *106*(D24), 33,867–33,889, doi:10.1029/2001JD900044.

Chen, F., and J. Dudhia (2001), Coupling an advanced land surface-hydrology model with the Penn State-NCAR MM5 modeling system. Part I. Model and implementation and sensitivity, *Mon. Weather Rev.*, *129*, 569–585, doi:10.1175/1520-0493(2001)129<0569:CAALSH>2.0.CO;2.

Chou, M.-D., and M. J. Suarez (1994), An efficient thermal infrared radiation parameterization for use in general circulation models, *NASA Tech. Memo., 104606*, 85 pp.

Comiso, J. (1999), Bootstrap sea ice concentrations from Nimbus-7 SMMR and DMSP SSM/I, January 1, 2007 to January 1, 2008, http://nsidc.org/data/nsidc-0079.html, Natl. Snow and Ice Data Cent., Boulder, Colo.

Dee, D., and S. Uppala (2008), Variational bias correction in ERA-Interim, *ECMWF Tech. Memo. 575*, 26 pp., ECMWF, Reading, U. K.

Dee, D. P., and S. Uppala (2009), Variational bias correction of satellite radiance data in the ERA- Interim reanalysis, *Q. J. R. Meteorol. Soc.*, *135*, 1830–1841, doi:10.1002/qj.493.

Durre, I., and X. Yin (2008), Enhanced radiosonde data for studies of vertical structure, *Bull. Am. Meteorol. Soc.*, *89*, 1257–1262, doi:10.1175/2008BAMS2603.1.

Elliott, W. P., and D. J. Gaffen (1991), On the utility of radiosonde humidity archives for climate studies, *Bull. Am. Meteorol. Soc.*, *72*, 1507–1520, doi:10.1175/1520-0477(1991)072<1507:OTUORH>2.0.CO;2.

Gemmill, W., B. Katz, and X. Li (2007), Daily real-time global sea surface temperature-high resolution analysis at NOAA/NCEP, *NOAA/NWS/NCEP/MMAB Office Note 260*, 39 pp., NOAA, Silver Spring, Md.

Grell, G. A., and D. Devenyi (2002), A generalized approach to parameterizing convection combining ensemble and data assimilation techniques, *Geophys. Res. Lett.*, *29*(14), 1693, doi:10.1029/2002GL015311.

Hines, K. M., and D. H. Bromwich (2008), Development and testing of Polar WRF Part I: Greenland ice sheet meteorology, *Mon. Weather Rev.*, *136*, 1971–1989, doi:10.1175/2007MWR2112.1.

Hines, K. M., D. H. Bromwich, L.-S. Bai, M. Barlage, and A. G. Slater (2011), Development and testing of Polar WRF: Part III. Arctic land, *J. Clim.*, *24*, 26–48, doi:10.1175/2010JCLI3460.1.

Hong, S.-Y., and J.-O. Lin (2006), The WRF single-moment 6-class microphysics scheme (WSM6), *J. Korean Meteorol. Soc.*, *42*(2), 129–151.

Inoue, J., J. Liu, J. O. Pinto, and J. Curry (2006), Intercomparison of Arctic regional climate models: Modeling clouds and radiation for SHEBA in May 1998, *J. Clim.*, *19*, 4167–4178, doi:10.1175/JCLI3854.1.

Janjić, Z. I. (2002), Nonsingular implementation of the Mellor-Yamada level 2.5 scheme in the NCEP Meso model, *NCEP Off. Note 437*, 61 pp., Natl. Cent. for Environ. Predict., Camp Springs, Md.

Kouraev, K., A. G. Kostianoy, and S. A. Lebedev (2009), Ice cover and sea level of the Aral Sea from satellite altimetry and radiometry (1992–2006), *J. Mar. Syst.*, *76*, 272–286, doi:10.1016/j.jmarsys.2008.03.016.

Lo, J. C.-F., Z.-L. Yang, and R. A. Pielke Sr. (2008), Assessment of three dynamical climate downscaling methods using the Weather Research and Forecasting (WRF) model, *J. Geophys. Res.*, *113*, D09112, doi:10.1029/2007JD009216.

Miloshevich, L. M., H. Vömel, A. Paukkenen, A. J. Haymsfield, and S. J. Oltmans (2001), Characterization and correction of relative humidity measurements from Vaisala RS80-A radiosondes at cold temperatures, *J. Atmos. Oceanic Technol.*, *18*, 135–156, doi:10.1175/1520-0426(2001)018<0135:CACORH>2.0.CO;2.

Mlawer, E. J., S. J. Taubman, P. D. Brown, M. J. Iacono, and S. A. Clough (1997), Radiative transfer for inhomogeneous atmosphere: RRTM, a validated correlated-k model for the longwave, *J. Geophys. Res.*, *102*(D14), 16,663–16,682, doi:10.1029/97JD00237.

Mooney, P. A., F. J. Mulligan, and R. Fealy (2010), Comparison of ERA-40, ERA-Interim and NCEP/NCAR reanalysis data with observed surface air temperature over Ireland, *Int. J. Clim.*, *31*, 487–632, doi:10.1002/joc.2098.

National Center for Atmospheric Research (1999), Dataset ds083.2: NCEP FNL operational model global tropospheric analyses, http://dss.ucar.edu/datasets/ds083.2, Boulder, Colo.

National Snow and Ice Data Center (2007), Arctic sea ice shatters all previous record lows, accessed 4 June 2009, http://nsidc.org/news/press/2007seaiceminimum/20071001pressrelease.html, Boulder, Colo.

Parish, T. R. (1992), On the interaction between Antarctic katabatic winds and tropospheric motions in the high southern latitudes, *Aust. Meteorol. Mag.*, *40*, 149–167.

Parish, T. R., and D. H. Bromwich (1991), Continental-scale simulation of the Antarctic katabatic wind regime, *J. Clim.*, *4*, 135–146, doi:10.1175/1520-0442(1991)004<0135:CSSOTA>2.0.CO;2.

Parish, T. R., and J. J. Cassano (2003), The role of katabatic winds on the Antarctic surface wind regime, *Mon. Weather Rev.*, *131*, 317–333, doi:10.1175/1520-0493(2003)131<0317:TROKWO>2.0.CO;2.

Parish, T. R., and K. T. Waight (1987), The forcing of Antarctic katabatic winds, *Mon. Weather Rev.*, *115*, 2214–2226, doi:10.1175/1520-0493(1987)115<2214:TFOAKW>2.0.CO;2.

Perovich, D. K., et al. (1999), Year on ice gives climate insights, *Eos Trans. AGU*, *80*(41), 481, 485–486.

Perovich, D. K., T. C. Grenfell, B. Light, and P. V. Hobbs (2002), Seasonal evolution of Arctic sea ice albedo, *J. Geophys. Res.*, *107*(C10), 8044, doi:10.1029/2000JC000438.

Perovich, D. K., S. V. Nghiem, T. Markus, and A. Schweiger (2007), Seasonal evolution and interannual variability of the local solar energy absorbed by the Arctic sea ice-ocean system, *J. Geophys. Res.*, *112*, C03005, doi:10.1029/2006JC003558.

Pinto, J. O., J. A. Curry, and C. W. Fairall (1997), Radiative characteristics of the Arctic atmosphere during spring as inferred from ground-based measurements, *J. Geophys. Res.*, *102*(D6), 6941–6952, doi:10.1029/96JD03348.

Powers, J. G., S. M. Cavallo, and K. W. Manning (2010), Improving upper-level performance in AMPS: Longwave radiation, *BPRC Tech. Rep. 2010–01*, pp. 56–61, Byrd Polar Res. Cent., Columbus, Ohio. (Available at http://polarmet.osu.edu/workshops/amomfw_2010/bprc_technical_report_2010-01.pdf.)

Ruffieux, D., P. O. G. Persson, C. W. Fairall, and D. E. Wolfe (1995), Ice pack and lead surface energy budgets during LEADEX 92, *J. Geophys. Res.*, *100*(C3), 4593–4612, doi:10.1029/94JC02485.

Shokr, M., A. Lambe, and T. Agnew (2008), A new algorithm (ECICE) to estimate ice concentration from remote sensing observations: An application to the 85-GHz passive microwave data, *IEEE Trans. Geosci. Remote Sens.*, *46*(12), 4104–4121, doi:10.1109/TGRS.2008.2000624.

Simmons, A., S. Uppala, D. Dee, and S. Kobayashi (2006), ERA-Interim: New ECMWF reanalysis products from 1989 onwards, *ECMWF Newsl.*, *110*, 25–35.

Skamarock, W. C., J. B. Klemp, J. Dudhia, D. Gill, D. Barker, M. Dudhia, X.-Y. Huang, W. Wang, and J. G. Powers (2008), A description of the Advanced Research WRF Version 3, *NCAR Tech. Note, NCAR/TN-475+STR*, 113 pp.

Uttal, T., et al. (2002), Surface heat budget of the Arctic Ocean, *Bull. Am. Meteorol. Soc.*, *83*, 255–275, doi:10.1175/1520-0477(2002)083<0255:SHBOTA>2.3.CO;2.

Zängl, G., and K. P. Hoinka (2001), The tropopause in the polar regions, *J. Clim.*, *14*, 3117–3139, doi:10.1175/1520-0442(2001)014<3117:TTITPR>2.0.CO;2.

D. H. Bromwich, K. M. Hines, and A. B. Wilson, Polar Meteorology Group, Byrd Polar Research Center, Ohio State University, 108 Scott Hall, 1090 Carmack Rd., Columbus, OH 43210, USA. (wilson.1010@buckeyemail.osu.edu)